Long heliostat facet with aluminium reflector structural panel analysis

Jean Schnaar-Campbell[1], Johann Bredell[2], and Craig McGregor[3]

[1] Stellenbosch University, Stellenbosch Central, Stellenbosch, South Africa; Phone: +27-742001865; E-Mail: 22862609@sun.ac.za

[2] Stellenbosch University; E-mail: jrbredell@sun.ac.za

[3] Stellenbosch University; E-mail: craigm@sun.ac.za

Abstract: Concentrating solar power (CSP) plants utilize reflective facets in heliostats to concentrate sunlight, but these facets contribute significantly to the cost of the plant. This study explores a novel heliostat facet design utilising long aluminium reflector panels to reduce costs. Three different support structure concepts for a 6 m long aluminium reflector facet are proposed and analysed: a frame support, a sandwich panel, and a formed sheet metal design. The facet concepts are compared based on their material costs and optical performance, quantified by the root mean square (RMS) slope error. Analytical calculations and finite element analysis are employed to determine the slope errors under representative loading conditions, including gravity and wind loads, at different facet angles. The results show that the frame-supported panel and formed sheet facets are the cheapest, and the formed sheet has the best optical performance. The sandwich panel is the most expensive and has the worst optical performance. This work demonstrates the potential of long aluminium reflector designs to reduce heliostat costs while maintaining optical performance, which could improve the economic viability of CSP plants.

Keywords: Concentrating solar power; heliostat facets; finite element analysis; sandwich panels; novel reflectors

1. Introduction

Worldwide there is an increasing demand for renewable electricity generation. However, the majority of renewable energy solutions are unreliable. Concentrating Solar Power (CSP) is capable of on-demand power generation [1]. In a traditional CSP plant, the reflective facets used are 7 % of the total cost of the plant [2]. The most common reflectors used in CSP plants are second surface silvered glass panels with a metal support structure. Alternate non-glass facets with a 25 % cost reduction potential have already been discovered [3] and developed for CSP applications [4].

This study focuses on a facet design for a polished aluminium reflector. The selected aluminium reflector is Alanod Miro-Sun [5]. This reflector is 0.5 mm thick with an above 95 % reflectivity, and a protective coating for weather resistance. Alonod Miro-Sun is sold as a long continuous roll of material. Long facets, like the one shown in Figure 1 have the potential for cost reduction due to the simpler support structure.

This study compares three different proposed designs for a long heliostat facet with a polished aluminium reflector. The designs are compared based on optical performance during operation and the cost of materials.

2. Methodology

First, a set of realistic design requirements had to be selected to generate viable facet designs. The design requirements were selected to create viable facets for a theoretical heliostat design and location. Once design requirements were selected, three heliostat concepts were generated, and their exact material compositions and dimensions were selected to fulfil all of the design requirements. The selected heliostats were compared based on theoretical slope errors and cost. Slope errors caused by construction and during operation were analysed separately, and combined into a single, net slope error.

2.1. Design Heliostat

Since no long heliostat facets exist currently, a new heliostat design was created. A simple heliostat design used in multiple CSP plants is a torque tube-based design. This was the base for the reference design selected. Existing heliostats' reflective area range is between 15 m^2 and 120 m^2 [4]. To allow the facets to be shipped in 6 m container, the facets length was set to 6 m. The width of each facet is set to 1.2 m, since most rolls of material have a width of 1.2 m - 1.25 m (source). The optimal aspect ratio of a heliostat facet should be close to 1.2 [6]. For the baseline heliostat, five facets were chosen, to set the aspect ratio to 1.0. Below is Figure 1, showing a sketch of the baseline heliostat.

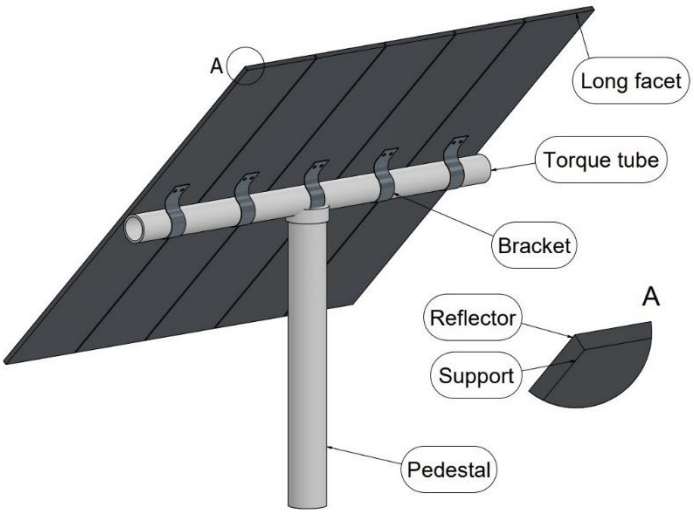

Figure 1: Baseline heliostat used for concept requirements

2.2. Facet Requirements

A set of design requirements was selected based on the baseline heliostat in Section 2.1, and weather data from Upington in South Africa (source). The overall facet dimensions, failure during operation from own weight and wind, failure during stow from wind and overall weight were considered for the requirements.

Table 1: Facet Requirements

ID	Requirement	Target	Unit
1	Facet length	6	m
2	Facet width	1.2	m
3	Operating wind speed	20	m/s
4	Own weight failure	False	Bool
5	Maximum deflection during operation	20	mm
6	Facet mass	100	kg
7	Stowed wind speed	44	m/s

2.3. Comparison Methodology

To compare the different concepts two factors are considered: material cost and net slope error. Material cost was calculated using the volume of material used for each facet and the bulk cost per unit volume of the respective material. Manufacturing costs were ignored since the cost of manufacturing was assumed similar between each concept.

The slope error was split into two components: slope error from manufacturing and slope error from operation. All concepts are assumed to be produced by placing the metal reflector on a paraboloid mandril and glueing the reflector in place. The slope error from manufacturing considers the slope error created from the elastic deformation that occurs after the reflector is removed from the mandril.

The operational slope error considers both the deformation from gravity and wind loads during operation. The weather data used is a typical meteorological year (TMY) generated by Sauran of Upington [7]. The deflection due to gravity is calculated using finite element analysis (FEA), considering the full range of elevation changes. Deformation due to wind loads is calculated using FEA and considering a handful of elevation angles. The peak and mean slope errors during operation are both used for comparison.

3. Concepts generation

Three viable concept facets were generated. The names given to each of the facets are: frame support, sandwich-panel and formed sheet.

3.1. Frame support

The frame-supported facet is based on some single-facet heliostats already proposed [8]. This facet features curved rectangular tubes welded together to create a frame. The reflective surface is glued to the frame while supported by a mandril. Below is Figure 2, showing a diagram of the frame-supported panel, with the frame in red and the reflector in grey.

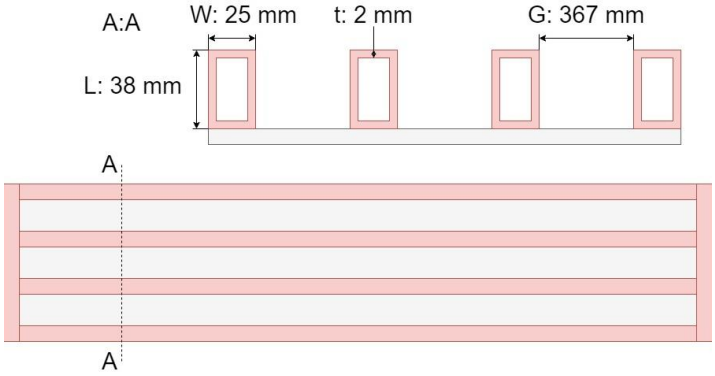

Figure 2: General structure of the frame-supported facet

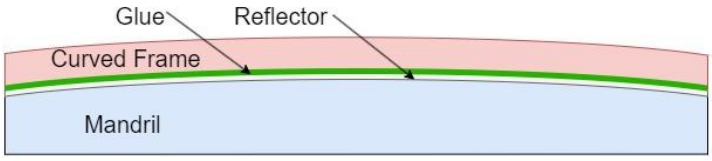

Figure 3: Frame-supported facet during construction

The spacing of the frame was selected based on an initial analytical calculation. A distributed load (q) of 119 Pa (based on the operating wind speed of 20 m/s) was placed on the panel, and its theoretical stress was calculated using Equation 1 from Roark's formulas for stress and strain (with β set to 0.75) [9].

The number of cross beams was increased till the maximum stress in the aluminium plate was lower than its yield stress. From this calculation, it was seen that 4 cross beams are required to support the aluminium reflector.

$$\sigma_{max} = \frac{\beta q G^2}{{t_{Al}}^2} \quad (1)$$

The required rectangular tube was selected based on the strength and stiffness requirements of the heliostat. Galvanised steel was selected as the material for the rectangular tube due to its low cost and corrosion resistance. To simplify calculations, the added mechanical strength from the reflective aluminium sheet was ignored. The limiting load case of the design was identified as deflection due to wind during operation, with the facet tilted at an angle of 90 ° (see Figure 6). The smallest rectangular tube that meets the 20 mm deflection requirement is a 38 mm x 25 mm tube.

From past experiments, Sikaflex Sikasil SG-20 was selected as the adhesive to attach the reflector to the rectangular tubing [10]. Sikasil SG-20 is ideal for this application since it is weather-resistant and compliant enough to allow for thermal expansion in the steel and aluminium. The glue can fill in a gap of up to 3 mm, meaning that any imperfections in the shaping of the square tube can be corrected during assembly. Figure 2 shows the final dimensions of the frame-supported face.

3.2. Sandwich-panel

The second concept was based on sandwich panels that have already been proposed for heliostat facets [11]. A sandwich panel is a panel made up of two skins (front and rear skins) and a core (see Figure 4). The sandwich layup is done on a mandril, with each component of the sandwich panel compliant enough to bend during layup, however becoming stiff when the glue is set.

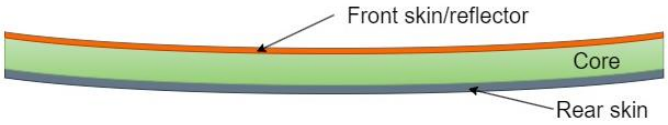

Figure 4: Sandwich panel

A study was done to select the materials and material thicknesses in the sandwich panel. In Microsoft Excel, the bending strength and stiffness were calculated analytically [12]. This was done using the composite material calculation in Chapter 8.2 of Roark's Formulas for Stress and Strain [9].

From Table 1, four criteria were identified as the minimum requirements for a viable facet. The panel must not yield or deflect more than 20 mm when exposed to the maximum operating wind speed of 20 m/s with the panel at 90 ° inclination and under its own weight at 0 ° inclination.

The mechanical properties of all solid materials from Ansys Granta Edupack [13] were exported to an Excel model that calculates the sandwich panel properties. The front skin was set to a 0.5 mm Aluminium. An automated script was written to iterate through all the combinations of core and rear skin materials and optimise each combination based on cost. The cost of the panel was calculated using the volume of material used and bulk material price exclusively. The cost and mechanical contribution of the glue layers were ignored.

All the material combinations were sorted in terms of price. The most optimal material combination is a 65 mm Polypropylene foam (0.02, closed cell) core with a 0.1 mm AISI 5140 rear skin. Polypropylene is uncommon in the South African market and was replaced with a Polyvinyl Chloride (PVC) (0.7, closed cell) core since this material is already mass-produced as insulating panels. AISI 5140 was replaced with galvanised mild steel for corrosion resistance, at a negligible extra cost. The final selected sandwich panel is described in Table 2.

Table 2: Optimal sandwich panel materials and properties

Component	Thickness [mm]	Cost [$/m^2]	Mass [kg/m^2]
Alanod	0.5	43.37	1.36
PVC foam	25	92.87	17.50
Mild steel	0.58	5.70	4.55

The selected adhesive for the sandwich panel is Ampreg 30 resin and 3X Slow hardener [14]. This is an epoxy resin system commonly used for creating sandwich panels. This was selected since the resin does not react with PVC and can easily be spread over the large area required.

3.3. Formed sheet

Formed sheets are stamped or rolled sheets of metal. Rolled metal sheets can be formed with a curved profile. The reflector is then glued to the formed sheet on top of a mandril. Formed sheets are already used in heliostat construction. An example is the HE54 heliostat by Senner, used for Noor III in Morocco [15]. The HE45 heliostat facet uses a stamped sheet to support and shape a 1 mm thick glass reflector.

To support a 6 m long heliostat facet a standard inverted box rib (IBR) sheet was selected. This is due to the existing large-scale infrastructure to create IBR sheets. Figure 5 shows a facet with an IBR sheet as the support.

Figure 5: Diagram of formed IBR sheet-based facet

Standard IBR sheets are generally made from galvanised steel sheets. The profile considered in this analysis is the IBR sheet sold by MacSteel [16]. MacSteel offers three different IBR sheet thicknesses. Each IBR sheet was tested against yield (ignoring the mechanical effects of the reflector and glue) in all the load cases mentioned in Table 1. The selected IBR sheet was 0.8 mm thick.

For the adhesive, Sikaflex Sikasil SG-20 was selected again for the same reasons as described in Section 3.1.

3.4. Costs

The cost of each facet is only considered as the cost of the materials required to construct the facet. The list and cost of materials for each concept are listed in Table 3 below.

Table 3: Final concepts materials and cost breakdown

Concept	Cost [$/m^2]	Mass [kg/m^2]
Frame support	52.64	7.53
Sandwich panel	141.93	23.41
IBR sheet	53.44	8.46

4. Operation error

The sources for significant material deflection during operation are gravitational loads and wind loads. Each of these sources of errors is analysed separately below, first using analytical methods, then finite element analysis (FEA).

The weather data used comes from the TMY created by Sauran for Upington South Africa [7]. The mean and maximum wind speeds are used for the analysis. The elevation angles are based on the worst load case and a common elevation angle of a typical heliostat field. The values considered for the analysis are in Table 4 below.

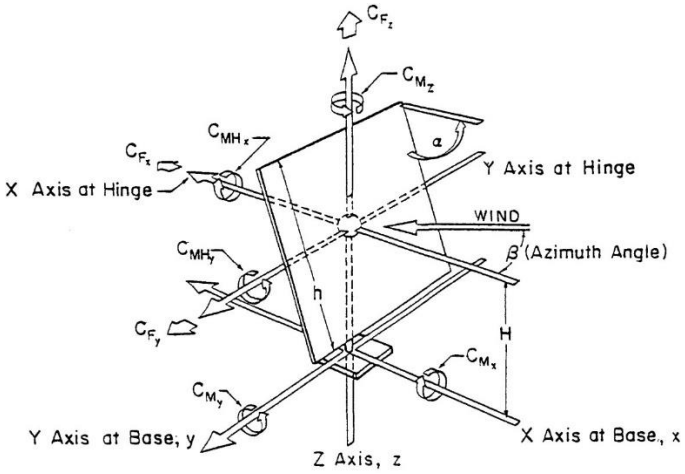

Figure 6: Loads and coordinate system used [17]

Table 4: Extreme and mean loads considered

No	Load	Angle (α) [°]	Magnitude
1	Wind mean	30	10 m/s
2	Wind max	90	20 m/s
3	Gravity mean	30	9.81 m/s^2
4	Gravity max	0	9.81 m/s^2

4.1. Analytical

Both analyses use the same method to convert from deflection to root mean square (RMS) slope error. RMS slope error is calculated by first calculating the flexure stiffness of the panel (including the reflector, excluding the glue). This is done by modelling all of the panels as a composite panel and then using Chapter 8.2 in Roark's Formulas for Stress and Strain to calculate the flexural stiffness.

The slope of the panel under load is calculated using beam theory. The arctan of the deformed slope is used to convert the slope into an angle in radians. Then Equation 2 is used to calculate the RMS slope error of the panel. The panels are all assumed flat initially, and the error is calculated relative to a perfectly flat profile.

$$RMS_x = \sqrt{\frac{x_1^2+x_2^2+x_3^2 \ldots + x_n^2}{n}} \quad (2)$$

The effect of gravity is modelled as a distributed load based on the materials' densities and dimensions. To consider the load at different angles, the cosine of gravitational acceleration is used. Below is Equation 3 showing the slope of the panel based on the tilt angle and mass of the heliostat.

$$TBD \quad (3)$$

According to A. Pfahl [6], the wind load on the heliostat can be calculated using tilt angle and wind speed. Below are Equation 4 and Equation 5 showing the force and moment caused by wind on a heliostat respectively. Both mean and peak force and moment coefficients were reported. For this study, the mean force and moment coefficients were used for load case 1, and peak coefficients were used for load case 2. The effect of wind is modelled using a combination of both factors creating a sloped distributed load. An example of the distributed load profile is shown in Figure 7.

$$F = C_F \frac{\rho}{2} v^2 A \quad (4)$$

$$M = C_M \frac{\rho}{2} v^2 A \quad (5)$$

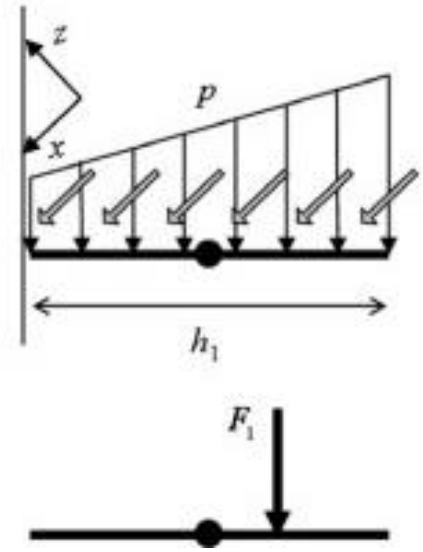

Figure 7: Equivalent distributed load from force and moment [6]

The slope errors for each concept are summarised in Table 5.

4.2. Numerical

To calculate the RMS slope error a finite element model was set up for each concept using Ansys Mechanical 2023 R2 [17].All three concepts were modelled using a quarter model meshed with shell elements. The same constraints are used for each load case, see Figure 8.

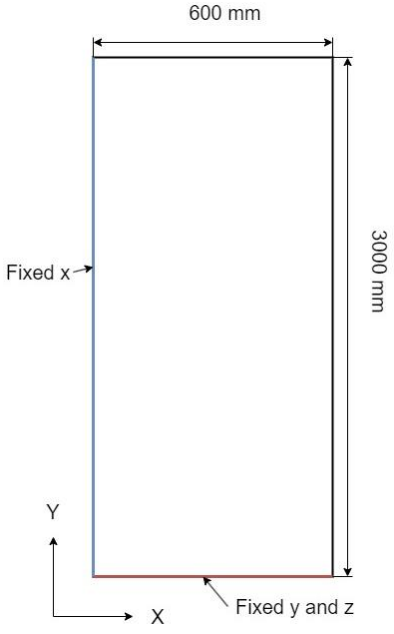

Figure 8: FEA model constrains

The sandwich panel model is created using composite elements with the materials and dimensions described in Table 2. The other two concepts used single material elements. All three models use flat reflectors.

The deformed point cloud of the model was extracted, and a structured grid of points was created by linear interpolation from the point cloud. The slopes in both x and y directions were calculated piecewise using the interpolated grid. The RMS errors were calculated using Equation 2. Below is an example heat map of the slope errors.

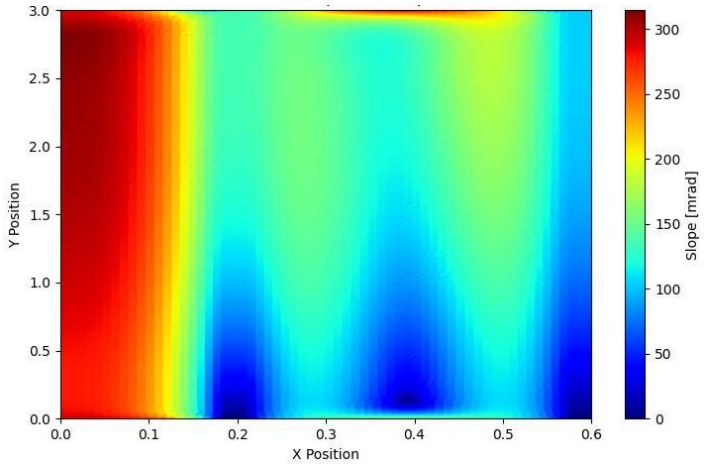

Figure 9: Slope error of frame facet load case 2

5. Comparison of results

Below are Table 5 and Table 6, showing the slope errors for each concept and load case. The net slope error is the sum of the slope error from cases 1 and 3 since this represents an expected slope error for a typical day.

Table 5: Analytical slope errors in each load case

Concept	RMS Slope error [mrad]				
	Case 1	Case 2	Case 3	Case 4	Net
Frame	0.3	3.92	2.11	2.436	2.41
Sandwich	2.46	10.23	17.04	19.68	19.5
IBR sheet	0.24	2.78	1.68	1.94	1.92

Table 6: Slope errors in each load case from FEA

Concept	RMS Slope error [mrad]				
	Case 1	Case 2	Case 3	Case 4	Net
Frame	33.60	352.64	17.03	20.50	50.63
Sandwich	3.67	122.85	77.02	88.93	80.70
IBR sheet	14.00	153.82	14.27	16.42	28.27

The results show that there is a significant difference between calculated analytical and FEA slope errors. Further investigation is required to solve the discrepancy. However, the relative performance of both analytical and FEA are similar.

The sandwich panel has a significantly worse performance than the other concepts, while also having the greatest cost of materials and mass. This is likely due to the density of the core.

Thicker and less dense foam cores will increase the stiffness and lower the weight of the panel. Further investigation is required to design a more optimal sandwich facet.

When comparing the other two concepts, the IBR sheet-supported facet has the best optical performance, while the frame-supported facet has around 30 % more slope error. Since the cost of the IBR sheet is marginally greater than the cost of the frame (Table 3), the best overall facet is the IBR sheet-supported facet.

6. Conclusion

This study analysed and compared three structural support concepts for long heliostat facets utilising an aluminium reflector: a frame support, sandwich panel, and formed inverted box rib (IBR) sheet. The facet designs were evaluated based on their material costs and optical performance, quantified by the root mean square (RMS) slope error under representative loading conditions.

The results showed that the IBR sheet-supported facet had the best overall performance, with the lowest net slope error and only marginally higher cost compared to the frame-supported design. The sandwich panel facet had significantly higher slope errors and material costs than the other two designs, likely due to the suboptimal density of the core material. Further optimisation of the sandwich panel could potentially improve its viability.

The discrepancy between the analytical and finite element analysis results for slope error requires additional investigation to resolve. However, the relative performance of the designs was consistent between the two methods.

In conclusion, this work demonstrates the potential of utilising formed IBR sheet metal to support long aluminium reflector facets in heliostats. This design approach can provide good optical performance while keeping material costs low, thereby contributing to the overall cost reduction and economic viability of concentrating solar power plants. Further research should explore optimising the sandwich panel design and resolving the analytical-numerical discrepancy in slope error calculations.

Acknowledgements

The authors acknowledge the financial support of the Solar Thermal Energy Research Group (STERG) at Stellenbosch University.

References

[1] World Bank, 'CONCENTRATING SOLAR POWER CLEAN POWER ON DEMAND 24/7', Washington, DC, 2020. Accessed: Aug. 12, 2024. [Online]. Available: https://pubdocs.worldbank.org/en/849341611761898393/WorldBank-CSP-Report-Concentrating-Solar-Power-Clean-Power-on-Demand-24-7-FINAL.pdf

[2] G. J. Kolb, C. K. Ho, T. R. Mancini, and J. A. Gary, 'SANDIA REPORT Power Tower Technology Roadmap and Cost Reduction Plan', 2011. [Online]. Available: http://www.ntis.gov/help/ordermethods.asp?loc=7-4-0#online

[3] J. Yellowhair and C. E. Andraka, 'Evaluation of advanced heliostat reflective facets on cost and performance', *Energy Procedia*, vol. 49, pp. 265–274, 2014, doi: 10.1016/j.egypro.2014.03.029.

[4] J. Coventry, J. Campbell, and C. J. Hall, 'Heliostat Cost Down Scoping Study-Final Report Ocean wave power View project Vortex tube View project', 2013. [Online]. Available: https://www.researchgate.net/publication/312214094

[5] Alanod, 'Alanod MIRO-SUN'. [Online]. Available: https://alanod.com/en/industries/solar/reflective-surfaces

[6] A. Pfahl, M. Buselmeier, and M. Zaschke, 'Wind loads on heliostats and photovoltaic trackers of various aspect ratios', *Solar Energy*, vol. 85, no. 9, pp. 2185–2201, Sep. 2011, doi: 10.1016/j.solener.2011.06.006.

[7] M. J. Brooks *et al.*, 'SAURAN: A new resource for solar radiometric data in Southern Africa', *Journal of Energy in Southern Africa*, vol. 26, no. 1, pp. 2–10, Mar. 2015, doi: 10.17159/2413-3051/2015/v26i1a2208.

[8] Schell, 'eSolar heliostat', *Solar Energy*, vol. 85, pp. 614–619, 2011.

[9] R. J. Roark, W. C. Young, and R. G. Budynas, *Roark's formulas for stress and strain*. McGraw-Hill, 2002.

[10] Sikaflex, 'Sikasil® SG-20'. Accessed: Sep. 22, 2024. [Online]. Available: https://industry.sika.com/dam/dms/au01/x/sikasil_sg-20.pdf

[11] STERG, 'Helio100 promises cost-effective solar power breakthrough', Sep. 2015. [Online]. Available: https://www.sun.ac.za/english/archive/Lists/English_News_Archive_110518/DispForm.aspx?ID=2863&ContentTypeId=0x010019F8BC5373DFA740B008FC720EA25DE601008842D5DFBB60F541BF61E7750F3D6BA5

[12] Microsoft Corporation, ‘Microsoft Excel’. [Online]. Available: https://office.microsoft.com/excel

[13] ANSYS Inc., ‘GRANTA EduPack’, 2023. [Online]. Available: www.ansys.com/materials

[14] AMT Composites, ‘Ampreg 30 Slow’. [Online]. Available: https://www.amtcomposites.co.za/product/ampreg-30-slow-6-3kg/

[15] S. Relloso and Y. Gutiérrez, ‘SENER molten salt tower technology. Ouarzazate NOOR III case’, in *AIP Conference Proceedings*, American Institute of Physics Inc., Sep. 2017. doi: 10.1063/1.4984384.

[16] MacSteel, ‘MacSteel IBR sheets’. Accessed: Sep. 23, 2024. [Online]. Available: https://macsteel.co.za/wp-content/uploads/2022/12/IBR-roofing-sheets-2021.pdf

[17] ANSYS Inc., ‘Ansys Mechanical 2023 R2’, 2023. [Online]. Available: https://www.ansys.com/products/structures/ansys-mechanical